Journal of Advanced Ceramics
2021, **10**(1): 28–38
https://doi.org/10.1007/s40145-020-0414-5

ISSN 2226-4108
CN 10-1154/TQ

Research Article

Microstructure and mechanical properties of 3D C_f/SiBCN composites fabricated by polymer infiltration and pyrolysis

Bowen CHEN[a,b,c,†], Qi DING[a,b,†], Dewei NI[a,b,*], Hongda WANG[a,b], Yusheng DING[a,b,*], Xiangyu ZHANG[a,b], Shaoming DONG[a,b,d]

[a] *State Key Laboratory of High Performance Ceramics and Superfine Microstructure, Shanghai Institute of Ceramics, Chinese Academy of Sciences, Shanghai 200050, China*
[b] *Structural Ceramics and Composites Engineering Research Center, Shanghai Institute of Ceramics, Chinese Academy of Sciences, Shanghai 200050, China*
[c] *University of Chinese Academy of Sciences, Beijing 100049, China*
[d] *Center of Materials Science and Optoelectronics Engineering, University of Chinese Academy of Sciences, Beijing 100049, China*

Received: May 29, 2020; Revised: August 5, 2020; Accepted: August 25, 2020

Abstract: In this work, three-dimensional (3D) C_f/SiBCN composites were fabricated by polymer infiltration and pyrolysis (PIP) with poly(methylvinyl)borosilazane as SiBCN precursor. The 3D microstructure evolution process of the composites was investigated by an advanced X-ray computed tomography (XCT). The effect of dicumyl peroxide (DCP) initiator addition on the crosslinking process, microstructure evolution, and mechanical properties of the composites were uncovered. With the addition of a DCP initiator, the liquid precursor can cross-linking to solid-state at 120 ℃. Moreover, DCP addition decreases the release of small molecule gas during pyrolysis, leading to an improved ceramic yield 4.67 times higher than that without DCP addition. After 7 PIP cycles, density and open porosity of the final C_f/SiBCN composite with DCP addition are 1.73 g·cm^{-3} and ~10%, respectively, which are 143.0% higher and 30.3% lower compared with the composites without DCP addition. As a result, the flexural strength and elastic modulus of C_f/SiBCN composites with DCP addition (371 MPa and 31 GPa) are 1.74 and 1.60 times higher than that without DCP addition (213 MPa and 19.4 GPa), respectively.

Keywords: C_f/SiBCN; ceramic matrix composites; dicumyl peroxide (DCP); X-ray computed tomography (XCT)

1 Introduction

Siliconboron carbonitride (SiBCN) ceramics have attracted considerable interests as their excellent thermal stability, high-temperature mechanical properties, and high creep resistance at elevated temperatures [1–4]. Based on these excellent properties, SiBCN ceramics are considered as a key candidate for applications under extreme conditions in the aerospace industry, such as the heat shield and leading edges of advanced aircraft [5–7]. However, low toughness and poor

† Bowen Chen and Qi Ding contributed equally to this work.
* Corresponding authors.
E-mail: D. Ni, deweini@mail.sic.ac.cn;
Y. Ding, ysding@mail.sic.ac.cn

thermal shock resistance restrict the wide application of SiBCN ceramics [8,9]. The C_f/SiBCN composites with carbon fiber as reinforcement fundamentally overcome the brittleness and poor thermal shock resistance, which are supposed to have a wider application in the above-mentioned areas [10–12].

Traditional methods for carbon fiber reinforced ceramic matrix composites fabrication include chemical vapor infiltration (CVI) [13–16], reactive melt infiltration (RMI) [17–21], pyrolysis (PIP) [22–26], etc. Due to the multicomponent of SiBCN, it is hard to obtain a SiBCN matrix by CVI or RMI. Up to now, most of the reported C_f/SiBCN composites are fabricated by PIP. Generally, a large amount of small-molecule gas is released during the pyrolysis process, which reduces the ceramic yield of precursor and decreases the fabrication efficiency of the composites [27–29]. Cross-linking of the precursor into large molecules has been proved to be an effective method to reduce the release of small molecules during pyrolysis. However, high cross-linking temperature (200 ℃ or even higher) and long cross-linking time (30 h) are generally required for the SiBCN precursor [30]. In our recent studies, it is reported that dicumyl peroxide (DCP) can be used as an effective initiator for the cross-linking of precursor [25,31–33]. It is indicated that DCP plays a significant role in the microstructure and further the properties of the final composites. However, the effect of DCP addition on the microstructure formation process and properties of the C_f/SiBCN composites has not been reported.

In this study, C_f/SiBCN composites were fabricated by the PIP method with and without DCP initiator addition. X-ray computed tomography (XCT) analysis was used to investigate the three-dimensional (3D) microstructure evolution of C_f/SiBCN composites. The effect of DCP initiator on the cross-linking behavior, microstructure evolution process, and mechanical properties was uncovered. This study will have a profound influence on the future advancement in design and fabrication technique and property improvement of C_f/SiBCN composites.

2 Experimental

3D needled carbon fibers (T700 3K, Toray, Tokyo, Japan) were used as the reinforcement of composites. The fiber fabrics with a density of 0.52 $g \cdot cm^{-3}$ and fiber volume fraction of about 28% were firstly deposited with the PyC interface by the CVI process [31]. Liquid poly(methylvinyl)borosilazane (PBSZ, Institute of Chemistry, Chinese Academy of Sciences, China) was used as the initial SiBCN precursor. 1 wt% dicumyl peroxide (DCP, Sinopharm Chemical Regeant Co., Ltd.) was added as a cross-linking initiator. The precursor was analyzed by Fourier transform infrared (FTIR) spectra (Tensor27, Bruker, Germany), thermogravimetric (STA 409/PC, Netzsch, Germany), and mass spectrometry (Advance III HD 500 MHz, Bruker, Germany). Using the PBSZ precursor with and without DCP addition, the SiBCN matrix was introduced into the 3D carbon fiber fabrics by vacuum impregnation, followed by cross-linking at 120 ℃ for 2 h. After that, the composites were pyrolyzed at 1100 ℃ for 2 h with a heating rate of 5 ℃/min in Ar atmosphere. With DCP addition, the C_f/SiBCN composites with an open porosity of ~10% were obtained after 7 PIP cycles. The density and open porosity of the prepared C_f/SiBCN composites were measured by the Archimedes' method using deionized water as an immersing medium.

The chemical composition of SiBCN ceramics was measured by the oxygen–nitrogen analyzer (TC600C, LECO, USA) and carbon–sulfur analyzer (CS2000, ELTRA, Germany). 3D microstructure evolution process of the as-fabricated C_f/SiBCN composites was analyzed by XTC (microXCT-400 Xradia, Inc. USA). Polished cross-sections and fracture surfaces of the composites were characterized by field emission scanning electron microscope (FE-SEM, Hitachi, S-4800, Tokyo, Japan). Flexural strength and elastic modulus of the composites were determined by a 3-point bending test (test bars: 4 mm × 6 mm × 60 mm) with a span of 50 mm and a loading rate of 0.5 mm/min. The reported value is an average of at least 5 valid measurements.

3 Results and discussion

3.1 Effect of DCP addition on the cross-linking behavior of PBSZ precursor

To determine the effect of DCP initiator on PBSZ precursor, both precursors with (PBSZ-D) and without DCP (PBSZ) were heat-treated at 120 ℃ for 2 h, which are labeled as PBSZ-D-120 and PBSZ-120, respectively. The as-treated precursor was measured by

TG analysis and *in-situ* mass spectrum. As shown in Fig. 1(a), the ceramic yield of PBSZ is only 15%. The *in-situ* mass spectra of PBSZ (Fig. 1(b)) indicate that the 80% mass loss at 200–300 ℃ can be attributed to the release of small molecule gas, including hydrogen, methane, ammonia, and ethylene. The ceramic yield of PBSZ-120 is similar to that of PBSZ (~15%). In comparison, the ceramic yield of PBSZ-D is ~30%. The ceramic yield of PBSZ-D-120 increases significantly to ~70%. The mass loss at 200–500 ℃ (5%) and 500–1000 ℃ (25%) are the two main regions in the TG curves of PBSZ-D-120. It should be noted that the precursor with DCP cross-links to a solid-state after heat-treatment at 120 ℃ for 2 h, but the precursor without DCP still presents as a liquid state (Fig. 2).

The molecular structural evolution of the precursors during cross-linking was investigated by FTIR spectrum (Fig. 3) for further analyzing the effect of DCP. Compared with PBSZ, no obvious change can be observed in that of PBSZ-120 (Fig. 3(a)). In contrast, the intensity of N–H (3429 cm^{-1}), $=CH_2$ (3177 cm^{-1}), =CH (3059 cm^{-1}), and C=C (1600 cm^{-1}) are significantly weaker with DCP addition. As $Si–CH_3$ is stable below 400 ℃ [34], the relative intensity of $(–CH=CH_2)/(Si–CH_3)$ can be used to evaluate the variation of $–CH=CH_2$. It shows that the relative intensity of $–CH=CH_2$ is reduced by ~86% after cross-linking at 120 ℃, indicating that about 86% of the $–CH=CH_2$ functional groups are reduced during the cross-linking process (Fig. 3(b)). In summary, the amount of vinyl functional groups can be distinctly reduced by adding DCP and cross-linking at 120 ℃, which significantly decreases the release of

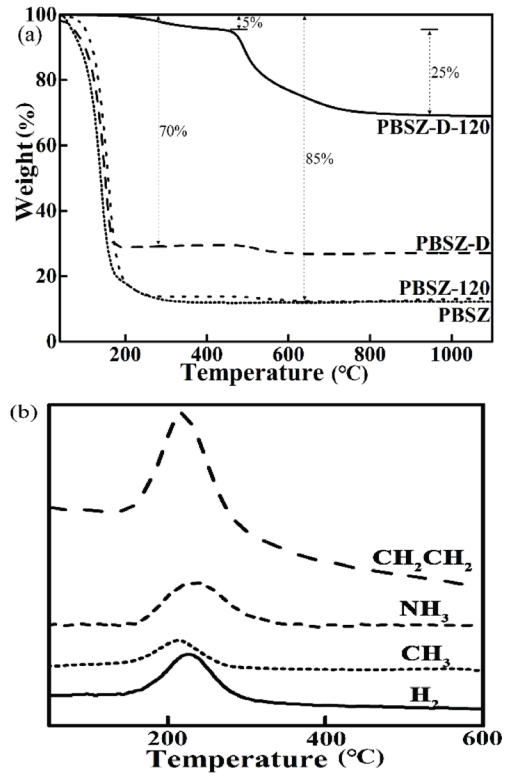

Fig. 1 (a) TG analysis curves of PBSZ, PBSZ-120, PBSZ-D, PBSZ-D-120 [31]; (b) mass spectrum (MS) curve of PBSZ during thermal treatment.

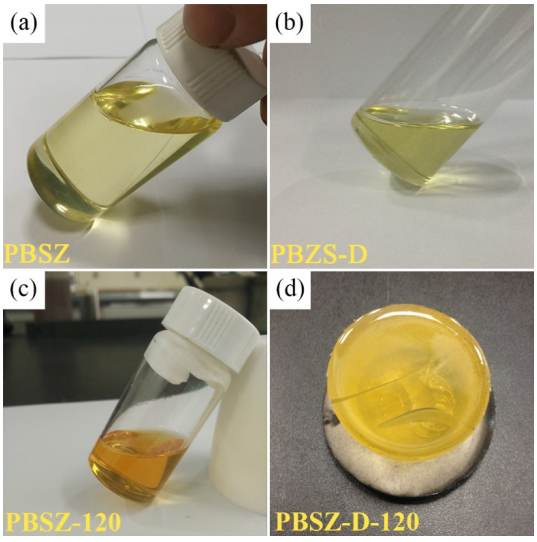

Fig. 2 Optical photographs of (a) PBSZ, (b) PBSZ-D, (c) PBSZ-120, and (d) PBSZ-D-120.

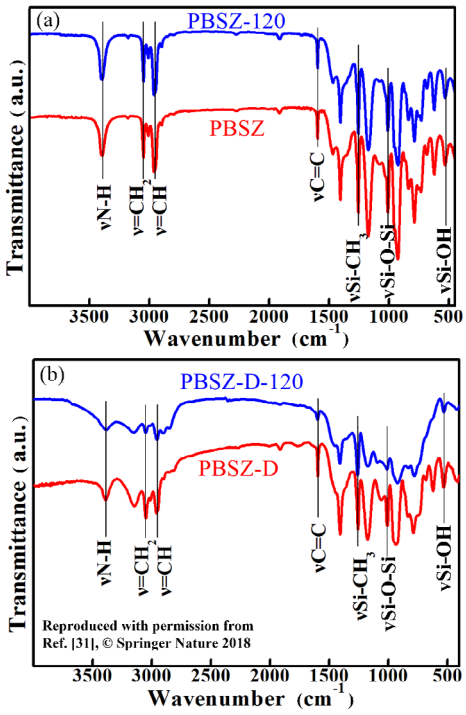

Fig. 3 FTIR spectra of (a) PBSZ and (b) PBSZ-D precursors before and after cross-linking [31].

small molecule gas and increases the ceramic yield.

XCT analysis was performed to reveal the microstructure difference between the pyrolyzed ceramics of PBSZ-120 and PBSZ-D-120, as shown in Fig. 4. After pyrolyzing at 1100 ℃, the PBSZ-120 is transformed into loose porous SiBCN ceramic (Fig. 4(a)) with a pore size of ~2 mm. During the pyrolysis process, the boiling precursor released small molecule gas (CH_4, NH_3, and $–CH=CH_2$) which formed the porous SiBCN ceramic. The volume shrinkage of the precursor during the pyrolysis process also resulted to form the porous SiBCN ceramic. In contrast, the solid-state of PBSZ-D-120 can maintain its shape during the pyrolysis process. Figure 4(b) shows that the pyrolysis product of PBSZ-D-120 presents a dense structure. Reticulate microcracks with a width of ~30 μm can be observed in the dense SiBCN ceramic. The microcracks are formed as the limited release of small molecule gas and the limited volume shrinkage during the cooling stage. The chemical composition of SiBCN ceramics with and without DCP addition was measured and the results were shown in Table 1. Due to the decrease content of –Si–O–Si and –Si–OH after adding DCP (Fig. 3), the oxygen impurity content of the SiBCN ceramics with DCP addition is 1.22%, which is less than that without DCP addition (4.16%).

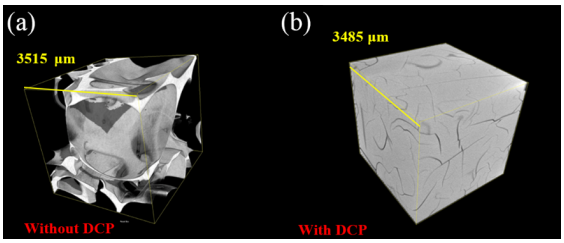

Fig. 4 μ-XCT images for pyrolysis product of (a) PBSZ-120 and (b) PBSZ-D-120.

Table 1 Chemical compositions of SiBCN ceramics with and without DCP addition [31]

Sample	Si	B	C	N	O
SiBCN (without DCP) (wt%)	44.52	7.05	27.64	16.63	4.16
SiBCN (with DCP) (wt%)	51.34	3.36	24.98	19.10	1.22

Therefore, the addition of DCP can reduce the oxygen impurity of the SiBCN ceramics.

3.2 Effect of DCP on microstructure evolution of C_f/SiBCN composites

Figure 5 shows the weight increase rate, density, and open porosity as a function of PIP cycles. All the composites were cross-linked at 120 ℃ for 2 h before pyrolysis for each PIP cycle. After the 1st PIP cycle, the weight of the composite impregnated by the precursor with DCP addition increased by 65.4% which is about 2.7 times higher than that without DCP (24.6%). This indicates that DCP addition increases the ceramic yield of precursor and improves the PIP efficiency of C_f/SiBCN composites significantly. After the 2nd PIP cycle, the weight increment of the composite with DCP addition (25.9%) is still higher than that without DCP (17.9%). However, from the 3rd PIP cycle, the weight increase of the composites without DCP addition is a little higher than that with DCP. This can be attributed to the less open porosity in the C_f/SiBCN composite with DCP addition. After 7 PIP cycles, the weight increase of the composite with DCP addition is lower than 1%, which is less than that without DCP (1.75%). The total weight increase of the C_f/SiBCN composite with DCP addition is about 166%, but that is only about 106% for the composite without DCP. The results indicate that after the entire PIP cycles, DCP addition to the precursor effectively improves the PIP

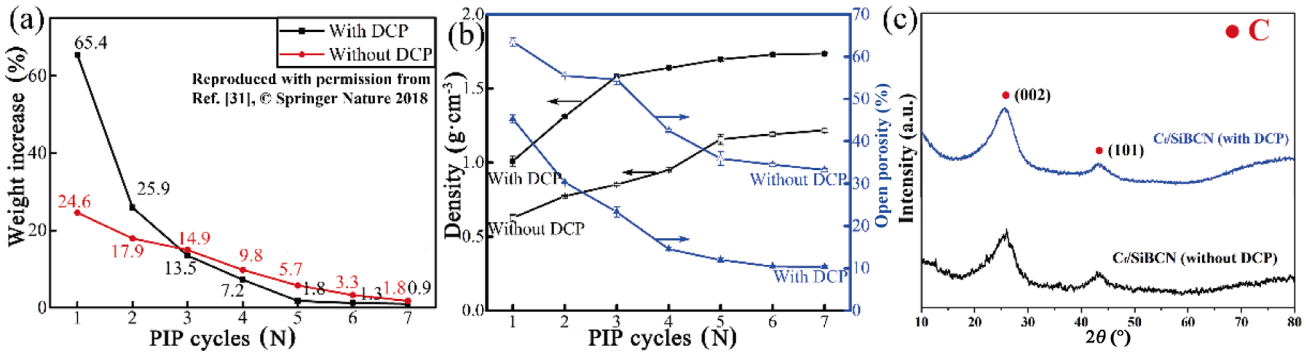

Fig. 5 (a) Weight increase rate curves [31], (b) density and open porosity variation curves of the composites as a function of PIP cycles, and (c) XRD patterns of the C_f/SiBCN composites with and without DCP addition.

efficiency of the C_f/SiBCN composite.

The effect of DCP on the density evolution of the C_f/SiBCN composite was also studied (Fig. 5(b)). The density of C_f/SiBCN with DCP addition is higher than that without DCP for each PIP cycle. After the 7th PIP cycle, the density of C_f/SiBCN composites with DCP addition is 1.73 g·cm^{-3}; however, the C_f/SiBCN composite without DCP addition is only 1.21 g·cm^{-3}. In contrast, the porosity of the C_f/SiBCN composites with DCP addition is always lower than that without DCP addition for each PIP cycle. After the 7th PIP cycle, the porosity of the C_f/SiBCN composite with DCP addition decreases to ~10%; however, that without DCP addition is ~33%. In summary, for the same PIP cycles, the addition of DCP can effectively increase the density of C_f/SiBCN composites and reduce their open porosity. The phase compositions of the C_f/SiBCN composites with and without DCP addition was determined by X-ray diffraction (XRD) and the results were shown in Fig. 5(c). The same peaks (at 26° and 43°) are observed in both composites corresponding to the (002) and (101) planes of carbon fiber. Otherwise, the SiBCN matrix in both composites is amorphous.

For further analyzing the microstructure evolution of the C_f/SiBCN composites, 3D visualization of the two C_f/SiBCN composites was performed by μ-XCT. XCT images in Figs. 6–8 show the densifying process of the two C_f/SiBCN composites. Figures 6(a), 6(c), 6(e), and 6(g) show the cross-section images of C_f/SiBCN without DCP addition after the 1st PIP cycle. Figures 6(a) and 6(c) show that the fiber preform contains 5 layers of *X*-direction fibers and 4 layers of

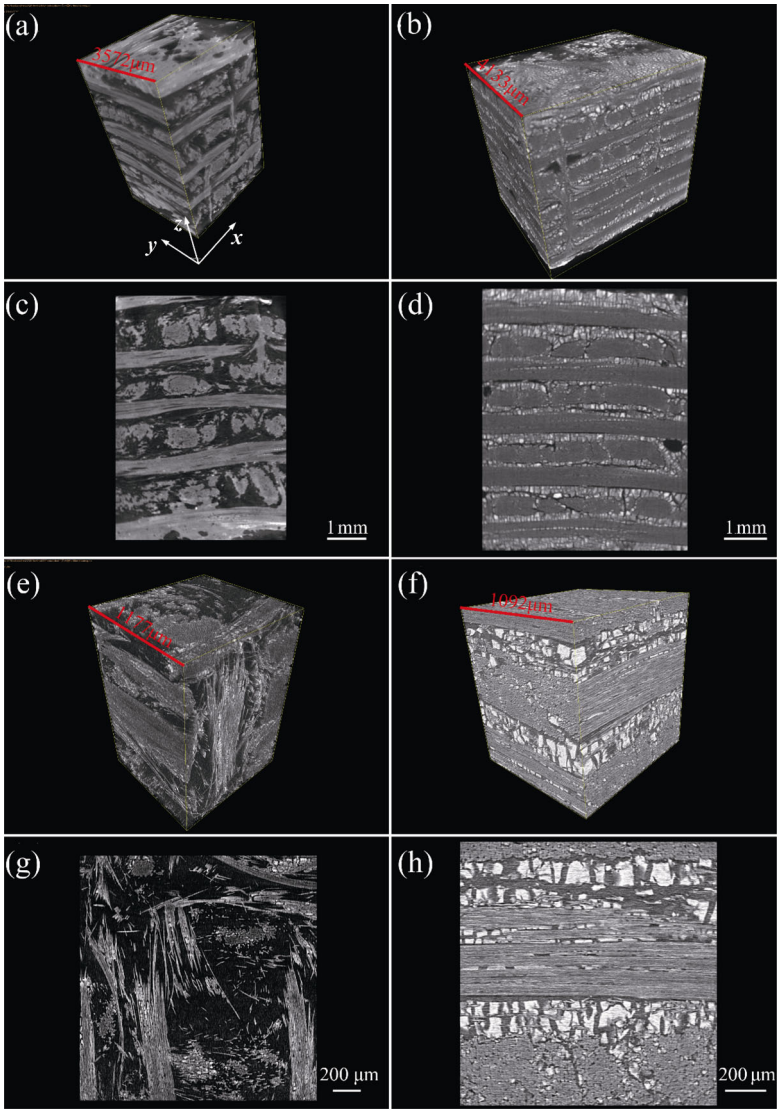

Fig. 6 XCT images of the C_f/SiBCN composites using (a, c, e, g) PBSZ and (b, d, f, h) PBSZ-D as the precursor after the 1st PIP cycle.

Y-direction fibers. The distance between the fiber bundles is about 200 μm. Limited SiBCN matrix can be observed between the fiber bundles. The high magnification images (Figs. 6(e) and 6(g)) show that a small amount of SiBCN matrix is filled in the fiber bundle. Figures 6(b), 6(d), 6(f) and 6(h) are cross-section images of the composite after the 1st PIP cycle using PBSZ-D as the precursor. Compared with Figs. 6(a) and 6(c), the composite in Figs. 6(b) and 6(d) has the same fiber arrangement. However, more SiBCN matrix can be found between the fiber bundles. The SiBCN matrix is divided into 100–200 μm fragmentized pieces by reticulate cracks (Figs. 6(f) and 6(h)). The fragmentized matrix structure is formed due to the volume shrinkage of the precursor during pyrolysis. And, the cracks can serve as channels for further precursor impregnation. With the increase of the impregnation times, these cracks will be slowly filled. However, large pores with a size of 300–500 μm are hard to be filled by precursors as this type of pores has limited capillary force for effective impregnation.

Figures 7(a), 7(c), 7(e), and 7(g) are the cross-sectional images of C_f/SiBCN without DCP addition after the 2nd PIP cycle, where the amount of SiBCN matrix is still very limited. From the higher magnification images (Figs. 7(e) and 7(g)), it can be seen that little amount of fragmented SiBCN matrix presents in the fiber bundles. Figures 7(b), 7(d), 7(f), and 7(h) are the cross-section images of C_f/SiBCN with DCP addition after the 2nd PIP cycle. The large pores in the matrix are still not filled (Figs. 7(b) and 7(d)). The higher magnification images (Figs. 7(f) and 7(h)) show that

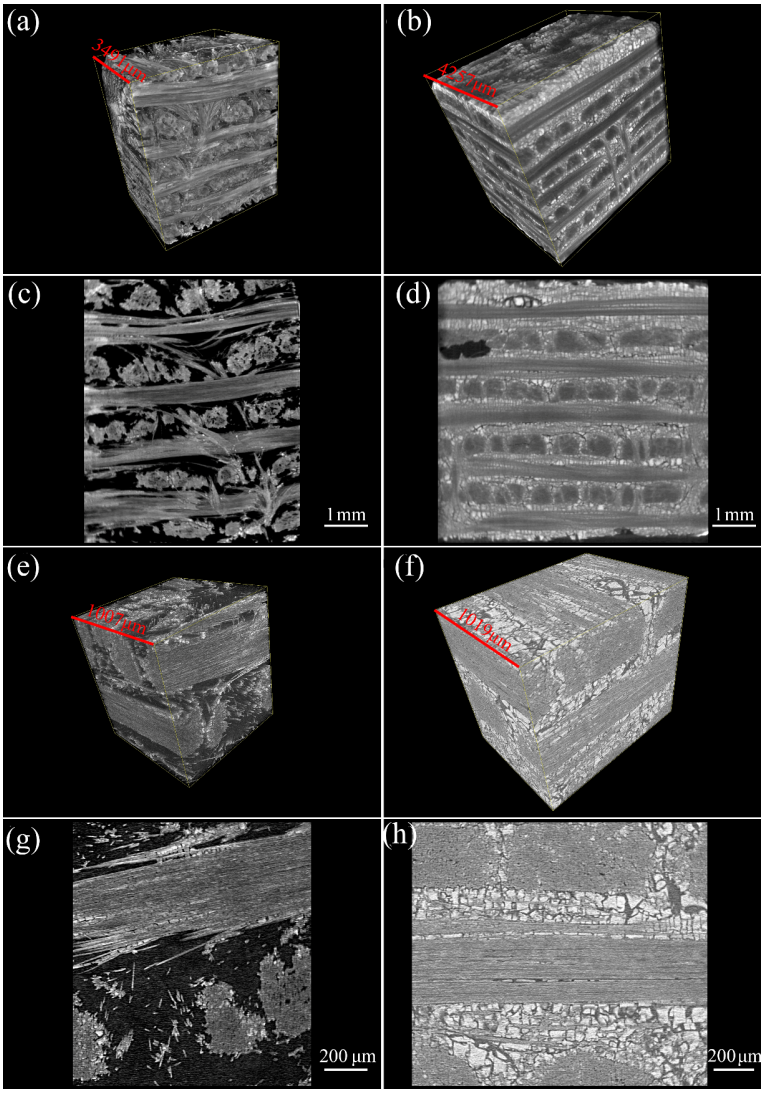

Fig. 7 XCT images of the C_f/SiBCN composites using (a, c, e, g) PBSZ and (b, d, f, h) PBSZ-D as the precursor after the 2nd PIP cycle.

both large and small SiBCN pieces exist in the matrix. Compared with the composite in Figs. 6(f) and 6(h), the size of the cracks is smaller in Figs. 7(f) and 7(h). This microstructure formed as the large cracks in Figs. 6(f) and 6(h) is filled by the small fragmented matrix. The large SiBCN pieces formed in the 1st PIP cycle and the small fragmented matrix is divided by small cracks during the 2nd PIP cycle.

Figures 8(a), 8(c), 8(e), and 8(g) are the cross-section images of C_f/SiBCN without DCP addition after the 7th PIP cycle. Many large pores still exist in the composite. Only a very limited SiBCN matrix can be found in the inter-bundle area even though the intra-bundle area is filled by the SiBCN matrix. In contrast, the composite with DCP has a dense SiBCN matrix both in the inter-bundle and intra-bundle area. On the other hand, the reticulate cracks are filled by the SiBCN matrix, only small pores and a limited number of cracks exist in the composite.

To sum up, the microstructure between the C_f/SiBCN composites is strongly influenced by DCP addition. As discussed above, the precursor without DCP addition cannot cross-link at low temperatures, which can flow out of the fiber preform before the pyrolysis process. As a result, less precursor in preform leading to the low matrix impregnation efficiency. On the other hand, the limited ceramic yield of the precursor also decreases the PIP efficiency. Consequently, the composite exhibits high porosity both in the inter-bundle and intra-bundle areas (Fig. 9(a)). In comparison,

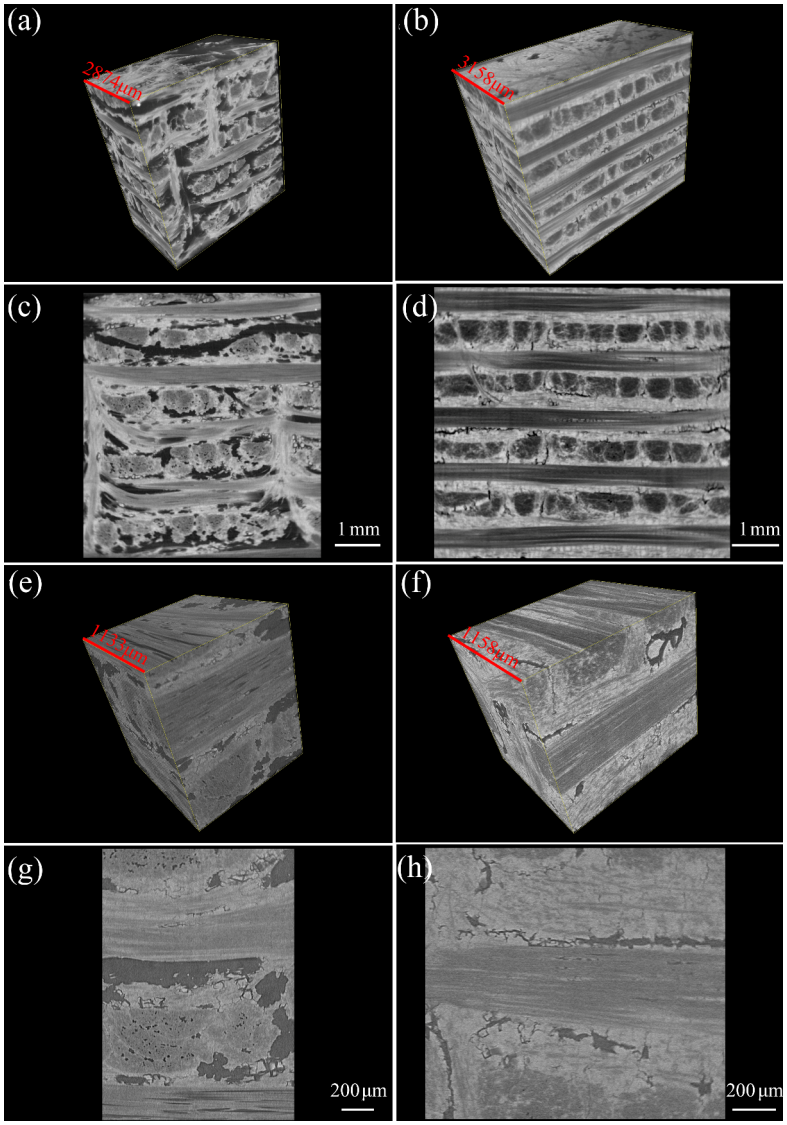

Fig. 8 XCT images of the C_f/SiBCN composites using (a, c, e, g) PBSZ and (b, d, f, h) PBSZ-D as the precursor after the 7th PIP cycle.

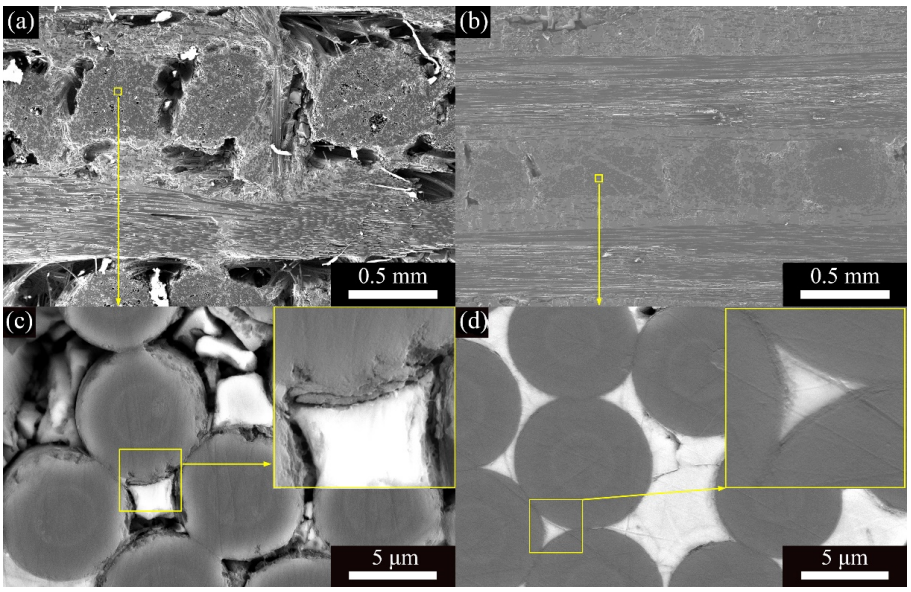

Fig. 9 SEM images of C_f/SiBCN composites using (a, c) PBSZ and (b, d) PBSZ-D as the precursor after the 7th PIP cycle.

the precursor with DCP addition can be introduced into fiber preform effectively. After cross-linking at 120 ℃, a large amount of the solid precursor is left in the preform. Benefiting from the high ceramic yield, dense SiBCN matrix is introduced into both inter-bundle and intra-bundle areas of the C_f/SiBCN composites (Fig. 9(b)).

3. 3 Mechanical properties of C_f/SiBCN composites

Mechanical properties of the two composites were determined by a 3-point bending test, and the stress–strain curves are shown in Fig. 10. Both curves exhibit obvious descending staircase characteristics, that is, the composites show a nonbrittle fracture behavior. Flexural strength and modulus of C_f/SiBCN composites with DCP addition are 371 MPa and 31 GPa, respectively, which increase by ~74% and 63% compared with the C_f/SiBCN composites without DCP addition (213 MPa and 19.4 GPa, respectively). Therefore, the addition of DCP greatly improves the mechanical properties of the C_f/SiBCN composites.

To reveal the relationship between mechanical properties and microstructure of C_f/SiBCN composites, the fracture morphology of the two composites is observed and shown in Fig. 11. In the C_f/SiBCN composites without DCP addition (Figs. 11(a) and 11(c)), a large amount of fibers break. However, less interface debonding and long fiber pull-out can be observed. In contrast, obvious fiber pull-out in the C_f/SiBCN composites with DCP addition (Figs. 11(b) and 11(d)), and the length of pull-out fibers is irregular. The microstructure indicates that

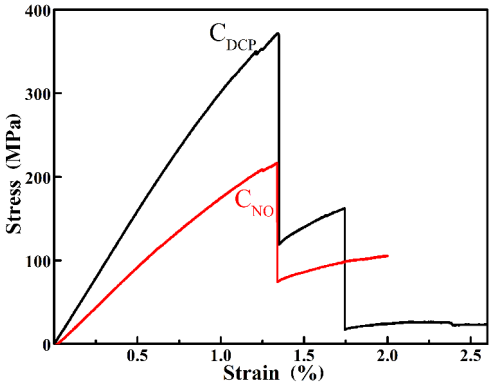

Fig. 10 Bending stress–strain curves of the two C_f/SiBCN composites with DCP addition (C_{DCP}) and without (C_{NO}).

the fibers in the C_f/SiBCN composites with DCP addition effectively deflect cracks. The cracks experience a long propagation path. This results in the outstanding mechanical properties of the C_f/SiBCN composites with DCP. The effect of DCP addition on different microstructures and mechanical properties of the composites can be summarized as follows:

1) The C_f/SiBCN composite without DCP addition has high porosity both in inter-bundle and intra-bundle areas, and the volume fraction of the SiBCN matrix is limited. The limited amount of matrix reduces the crack deflection path in composite and the stress accumulates on fibers. Almost only carbon fibers bear and transmit the load during the bending test. On the other hand, the vast volume shrinkage of the SiBCN matrix without DCP addition during the pyrolysis process

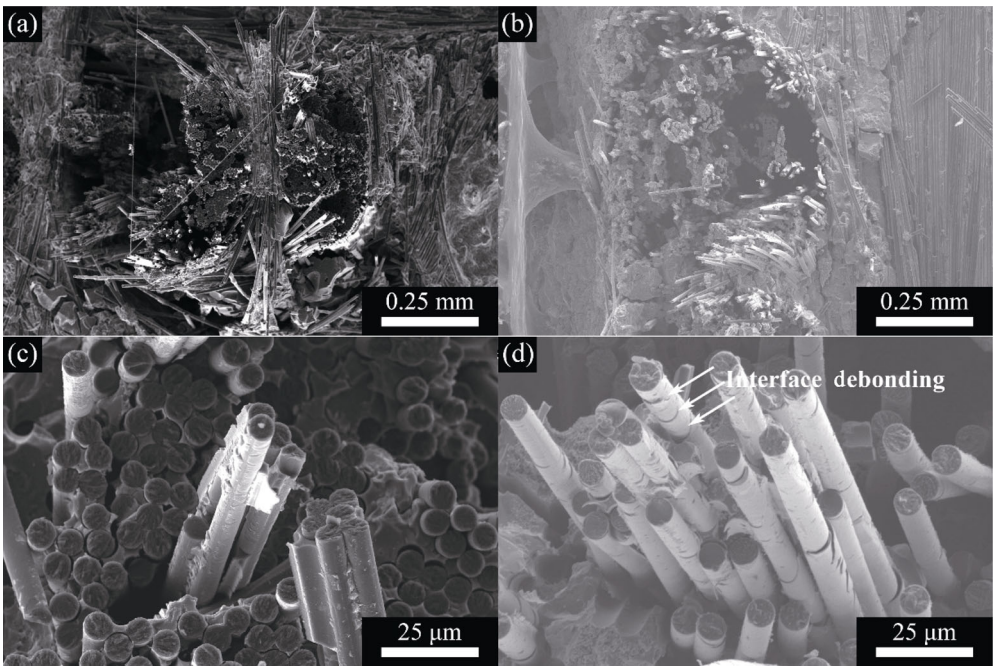

Fig. 11 SEM images of fracture morphology of two C_f/SiBCN composites: (a, c) C_f/SiBCN without DCP addition and (b, d) C_f/SiBCN with DCP addition.

leading to the damage of the PyC interface. The PyC interface falls off from the carbon fibers (Fig. 9(c)) which reduces the amount of interface debonding during the bending test. Consequently, with the increase of load, fibers break resulting in the fracture of the composite.

2) The C_f/SiBCN composite has low porosity and dense matrix both in inter-bundle and intra-bundle areas benefiting from the addition of DCP. During the bending test, the matrix bears the bending load and transmits the load to the fibers. The vast amount of dense SiBCN matrix provides a sufficient path for crack deflection in the composite. The intact PyC interface exists between carbon fibers and the dense SiBCN matrix (Fig. 9(d)) which also provides the crack deflection path. The cracks firstly form, then, propagate in the matrix and deflect at the interface, which reduce the crack propagation energy. Fibers break with the increase of the load accumulation. Due to the sufficient dense matrix around fibers, the broken fibers effectively pull-out from the matrix, which also reduce the energy of crack propagation. As a result, the composite exhibits better mechanical properties.

4 Conclusions

In this study, 3D C_f/SiBCN composites were fabricated by PIP with poly(methylvinyl)borosilazane as SiBCN precursor. The 3D microstructure evolution process of the composites was investigated by an advanced XCT. The effect of DCP initiator addition on the cross-linking process, microstructure evolution, and mechanical properties of the composites was revealed. With the addition of a DCP initiator, the liquid precursor can cross-link to solid-state at 120 ℃. Moreover, the DCP addition decreases the release of small molecule gas which increases the ceramic yield by 4.67 times higher than that without DCP addition. After 7 PIP processes, the density and the open porosity of the final composite with DCP addition are 1.73 $g \cdot cm^{-3}$ and ~10%, respectively, which are 142.98% higher and 30.30% lower than those of composite without DCP addition. An intact PyC interface exists in the C_f/SiBCN composites with DCP addition. As a result, the flexural strength and modulus of C_f/SiBCN composites with DCP addition are 371 MPa and 31 GPa, respectively, which are 1.74 and 1.60 times higher than those of the C_f/SiBCN composites without DCP addition (213 MPa and 19.4 GPa, respectively).

Acknowledgements

The financial support from the National Key Research and Development Program of China (2016YFB0700202), the Key Research Program of Frontier Sciences, CAS

(QYZDY-SSW-JSC031), the National Natural Science Foundation of China (51702341 and 51872310), and the project supported by State Key Laboratory of Advanced Technology for Materials Synthesis and Processing (Wuhan University of Technology, 2021-KF-5) are greatly acknowledged.

References

[1] Riedel R, Kienzle A, Dressler W, *et al*. A silicoboron carbonitride ceramic stable to 2000 ℃. *Nature* 1996, **382**: 796–798.

[2] Christ M, Thurn G, Weinmann M, *et al*. High-temperature mechanical properties of Si–B–C–N-precursor-derived amorphous ceramics and the applicability of deformation models developed for metallic glasses. *J Am Ceram Soc* 2000, **83**: 3025–3032.

[3] Kumar NVR, Prinz S, Cai Y, *et al.* Crystallization and creep behavior of Si–B–C–N ceramics. *Acta Mater* 2005 **53**: 4567–4578.

[4] Schmidt H, Gruber W, Borchardt G, *et al*. Coarsening of nano-crystalline SiC in amorphous Si–B–C–N. *J Eur Ceram Soc* 2005, **25**: 227–231.

[5] Yang ZH, Jia DC, Duan XM, *et al*. Effect of Si/C ratio and their content on the microstructure and properties of Si–B–C–N Ceramics prepared by spark plasma sintering techniques. *Mater Sci Eng: A* 2011, **528**: 1944–1948.

[6] Aldinger F, Weinmann M, Bill J. Precursor-derived Si–B–C–N ceramics. *Pure Appl Chem* 1998, **70**: 439–448.

[7] Ding Q, Ni DW, Ni N, *et al*. Thermal damage and microstructure evolution mechanisms of C_f/SiBCN composites during plasma ablation. *Corros Sci* 2020, **169**: 108621.

[8] Jia DC, Liang B, Yang ZH, *et al*. Metastable Si–B–C–N ceramics and their matrix composites developed by inorganic route based on mechanical alloying: Fabrication, microstructures, properties and their relevant basic scientific issues. *Prog Mater Sci* 2018, **98**: 1–67.

[9] Ding Q, Ni DW, Wang Z, *et al*. Effect of interphase on mechanical properties and microstructures of 3D C_f/SiBCN composites at elevated temperatures. *J Am Ceram Soc* 2019, **102**: 3630–3640.

[10] Evans AG. Perspective on the development of high-toughness ceramics. *J Am Ceram Soc* 1990, **73**: 187–206.

[11] Besmann TM, Sheldon BW, Lowden RA, *et al*. Vapor-phase fabrication and properties of continuous-filament ceramic composites. *Science* 1991, **253**: 1104–1109.

[12] Zhao H, Chen LX, Luan XG, *et al*. Synthesis, pyrolysis of a novel liquid SiBCN ceramic precursor and its application in ceramic matrix composites. *J Eur Ceram Soc* 2017, **37**: 1321–1329.

[13] Naslain R. Design, preparation and properties of non-oxide CMCs for application in engines and nuclear reactors: An overview. *Compos Sci Technol* 2004, **64**: 155–170.

[14] Wang HD, Feng Q, Wang Z, *et al*. The corrosion behavior of CVI SiC matrix in SiC_f/SiC composites under molten fluoride salt environment. *J Nucl Mater* 2017, **487**: 43–49.

[15] Ma XK, Yin XW, Cao XY, *et al*. Effect of heat treatment on the mechanical properties of SiC_f/BN/SiC fabricated by CVI. *Ceram Int* 2016, **42**: 3652–3658.

[16] Feng W, Zhang LT, Liu YS, *et al*. Thermal and mechanical properties of SiC/SiC–CNTs composites fabricated by CVI combined with electrophoretic deposition. *Mater Sci Eng: A* 2015, **626**: 500–504.

[17] Chen BW, Ni DW, Wang JX, *et al*. Ablation behavior of C_f/ZrC–SiC-based composites fabricated by an improved reactive melt infiltration. *J Eur Ceram Soc* 2019, **39**: 4617–4624.

[18] Kim SY, Han IS, Woo SK, *et al*. Wear-mechanical properties of filler-added liquid silicon infiltration C/C–SiC composites. *Mater Des* 2013, **44**: 107–113.

[19] Zhong Q, Zhang XY, Dong SM, *et al*. Reactive melt infiltrated C_f/SiC composites with robust matrix derived from novel engineered pyrolytic carbon structure. *Ceram Int* 2017, **43**: 5832–5836.

[20] Chen XW, Dong SM, Kan YM, *et al*. 3D C_f/SiC–ZrC–ZrB_2 composites fabricated via sol-gel process combined with reactive melt infiltration. *J Eur Ceram Soc* 2016, **36**: 3607–3613.

[21] Chen XW, Dong SM, Kan YM, *et al*. Microstructure and mechanical properties of three dimensional C_f/SiC–ZrC–ZrB_2 composites prepared by reactive melt infiltration method. *J Eur Ceram Soc* 2016, **36**: 3969–3976.

[22] Lee SH, Weinmann M, Aldinger F. Processing and properties of C/Si–B–C–N fiber-reinforced ceramic matrix composites prepared by precursor impregnation and pyrolysis. *Acta Mater* 2008, **56**: 1529–1538.

[23] Weinmann M, Kamphowe TW, Schuhmacher J, *et al*. Design of polymeric Si–B–C–N ceramic precursors for application in fiber-reinforced composite materials. *Chemistry of Materials* 2000, **12**: 2112–2122.

[24] Li KZ, Xie J, Li HJ, *et al*. Ablative and mechanical properties of C/C–ZrC composites prepared by precursor infiltration and pyrolysis process. *J Mater Sci Technol* 2015, **31**: 77–82.

[25] Zhong H, Wang Z, Zhou HJ, *et al*. Properties and microstructure evolution of C_f/SiC composites fabricated by polymer impregnation and pyrolysis (PIP) with liquid polycarbosilane. *Ceram Int* 2017, **43**: 7387–7392.

[26] Kannan R, Rangaraj L. Properties of C_f/SiC–ZrB_2–Ta_xC_y composite produced by reactive hot pressing and polymer impregnation pyrolysis (RHP/PIP). *J Eur Ceram Soc* 2019, **39**: 2257–2265.

[27] Li YL, Kroke E, Riedel R, *et al*. Thermal cross-linking and pyrolytic conversion of poly(ureamethylvinyl)silazanes to silicon-based ceramics. *Appl Organometal Chem* 2001, **15**: 820–832.

[28] Yajima S, Shishido T, Kayano H, *et al*. SiC sintered bodies with three-dimensional polycarbosilane as binder. *Nature*

1976, **264**: 238–239.

[29] D'Elia R, Dusserre G, del Confetto S, *et al*. Cure kinetics of a polysilazane system: Experimental characterization and numerical modelling. *Eur Polym J* 2016, **76**: 40–52.

[30] Lee SH, Weinmann M, Aldinger F. Processing and properties of C/Si–B–C–N fiber-reinforced ceramic matrix composites prepared by precursor impregnation and pyrolysis. *Acta Mater* 2008, **56**: 1529–1538.

[31] Ding Q, Ni DW, Wang Z, *et al*. 3D C_f/SiBCN composites prepared by an improved polymer infiltration and pyrolysis. *J Adv Ceram* 2018, **7**: 266–275.

[32] Konegger T, Patidar R, Bordia RK. A novel processing approach for free-standing porous non-oxide ceramic supports from polycarbosilane and polysilazane precursors. *J Eur Ceram Soc* 2015, **35**: 2679–2683.

[33] Wang LH, Luo YM, Xu CH, *et al.* Studies on curing reaction kinetics of liquid polycarbosilane. *Polym Bull* 2016, (9**)**: 149–155. (in Chinese)

[34] Yu ZJ, Yang L, Min H, *et al*. Single-source-precursor synthesis of high temperature stable SiC/C/Fe nanocomposites from a processable hyperbranched polyferrocenylcarbosilane with high ceramic yield. *J Mater Chem C* 2014, **2**: 1057–1067.